Modern Physical Chemistry Research (2024)
Clausius Scientific Press, Canada

DOI: 10.23977/mpcr.2024.040111
ISSN 2616-1702 Vol. 4 Num. 1

Numerical study of viscous fingering patterns under annular boundaries based on the Hele-Shaw model

Jingying Wei

School of Applied Physics, Chengdu University of Technology, Chengdu, 610059, China

Keywords: Fractal Finger, Viscous Fingering, Hele-Shaw, Annular Boundary

Abstract: In porous media, when a low-viscosity fluid displaces a high-viscosity fluid, the phenomenon of viscous fingering is formed due to the instability and nonlinear effect at the interface of the two phases, which exhibits a complex branching structure and self-similarity. In numerical simulations, the Hele-Shaw model is often used to simulate the replacement phenomenon in porous media, and the fractal evolution of viscous fingering can also be observed. Based on the two-phase Darcy's law, this paper investigates the influence parameters and fractal differences related to the Hele-Shaw model for the radial injection of miscible two-phase under an annular boundary, in terms of the spreading area and the boundary length. The analytical results show that with the increase in log-viscosity ratio, a tendency of more elongated finger structures and a consequent increase in the number of bifurcations of the main branches are observed. Meanwhile, the decrease in diffusion coefficient led to a more complex fractal structure and further enhanced the splitting effect. In addition, the higher injection rate of the replacement fluid extends the spreading range of the interface, which increases the complexity of the finger structure and the number of "fingers". These results highlight the significant influence of convection and diffusion parameters on the morphology and dynamics of multiphase fluid interfaces and provide important theoretical support for understanding and controlling related engineering and environmental processes.

1. Introduction

Viscous fingering is a fractal pattern similar to "fingers" produced by interfacial instability when a less viscous fluid replaces a more viscous one, and this phenomenon is widely found in seepage studies in the petroleum industry, nature, chemical engineering, and groundwater management, etc. The study of viscous fingering can be traced back to the work of Saffman and Taylor[1] in 1958, who analyzed the Hele-Shaw model with two parallel plates.

The study of viscous finger inlet due to interfacial instability can be traced back to the work of Saffman and Taylor in 1958, which analyzed the finger inlet phenomenon under the Hele-Shaw model consisting of two parallel flat plates, and thus developed an important research field. Viscous fingering can be divided into immiscible and miscible viscous fingering. Immiscible viscous fingering is often described by Ca numbers, which are characterized by the interfacial tension interaction of viscous forces. Unlike miscible viscous fingering, however, due to the absence of interfacial tension and the influence of buoyancy-driven convection in a gravitational field, it is often described by the

Pe number, which is characterized by the competing mechanisms of convection and diffusion. Miscible fluids have been studied extensively, for example, Pramanik and Mishara[2] et al. investigated the variability of growth rates between liquid phases in the two cases of high viscosity replacing low viscosity and low viscosity replacing high viscosity, and Deki[] et al. analyzed the effect of Pe on viscous fingering in the presence and absence of effective interfacial tension (EIT), among others. effects, etc.

Research indicates a lack of studies on the graphical complexity of fractal fingers. Consequently, this paper utilizes COMSOL Multiphysics, a powerful multi-physics simulation software, to simulate radial injection into an annular boundary. This simulation employs the Two-phase Darcy Law (TPDL) module of the Hele-Shaw model, drawing on the work of Sharma[4,5] and other researchers. By adjusting parameters such as log-viscosity ratio, injection velocity, and diffusion coefficient, this study analyzes the formation, growth, and interaction of finger-like structures. The results aim to provide a reference for the control and application of fluid transport.

2. Mathematical model and control equations

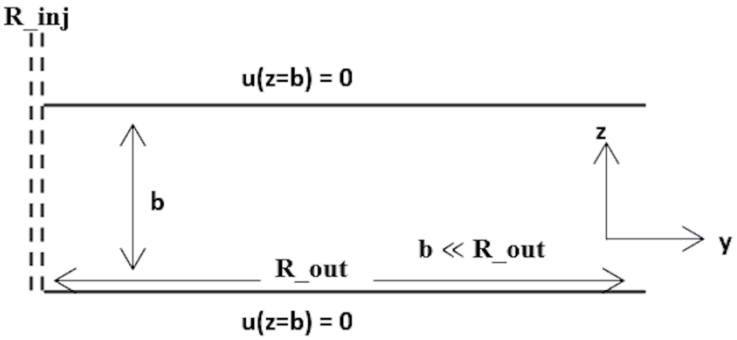

Figure 1: Side view of the Hele-Shaw model

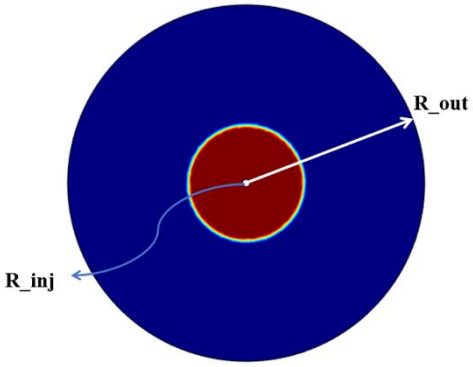

Figure 2: Hele-Shaw model with annular boundary

Figure 1 shows a side view of the Hele-Shaw model in 3D. As shown in Figure 2, let the driven fluid occupy the whole circular plate region, the radius of the circular domain of the driven fluid is R_out, the driven fluid is injected from a small hole with radius R_inj, and the thickness between the parallel circular plates is b, where the thickness b between the two plates is much smaller than the radius of the circular plate.

Considering the expelling and expelled fluids as mutually miscible incompressible Newtonian fluids, the following equations can be obtained[4,5]:

Continuity equation:

$$\nabla \bullet u = 0 \tag{1}$$

Darcy's law satisfied by the Hele-Shaw model can be obtained from the N-S equation and the boundary conditions between the two plates:

$$u = -\frac{b^2}{12\mu}\nabla P \tag{2}$$

Convection-diffusion equation:

$$\frac{\partial \varepsilon c}{\partial t} + u \cdot \nabla c - D \cdot \nabla^2 c = 0 \tag{3}$$

u is the flow rate of the flow field, c is the concentration of the replacement fluid, ε is the permeability of the replacement fluid, and D is the diffusion coefficient. The second term of the equation describes the diffusion effect of the substance, and the third term describes the convection effect of the substance as it moves with the flow field.

$$\frac{1}{\mu} = s_1 \frac{\kappa_1}{\mu_1} + s_2 \frac{\kappa_2}{\mu_2} \tag{4}$$

Set the log-viscosity ratio to $R = \ln \frac{\mu_1}{\mu_2}$ where μ_1 is the dynamic viscosity of displacing fluid, μ_2 is the dynamic viscosity of the displaced fluid. κ_1, κ_2 is the permeability of the two phases. s_1, s_2 is the two-phase saturation,which characterizes the effect of viscosity difference between two-phase miscible fluids on the fractal evolution, where s_1, s_2 can also characterize the two−phase angularly averaged concentration denoted as $\langle s_1 \rangle, \langle s_2 \rangle$. Assuming that $\kappa_1 = \kappa_2 = 1$ and $\mu_1 = \mu_2 e^R$. Then the above equation becomes:

$$\frac{1}{\mu} = \frac{1}{\mu_2}\left(1 + e^{-R}\right)\left(s_1 + s_2\right) \tag{5}$$

$$s_1 + s_2 = 1 \tag{6}$$

According to $c_1 = \rho_1 s_1$, $c_2 = \rho_2 s_2 = \left(1 - s_1\right)\rho_2$ the centration values of the two phases can be calculated during the displacement process.

3. Numerical simulation analysis

The generation of fractal phenomena is inextricably linked to the competing mechanisms of diffusion and convection. In the case of miscible fluids, the replacement fluid is injected into the substrate fluid and continuously diffuses outward in a complementary manner, forming a dynamic interface at the junction. The initially formed dynamic interface meets the replenishment fluid, and both the diffusion of solutes and the increase of the concentration number lead to an increase in the fractal dimension, which in turn indicates an increase in the complexity of the system during the rejection process.

Under the action of concentration gradient, the dynamic joint interface is destabilized, and the first intrusion at the favorable flow of the repellent liquid will form a perturbing quantity to the interface, which makes the interface move in the form of ripples, and the cycle is repeated. After reaching a certain threshold, a convex split is formed at the ripples, forming a fractal fork structure, making the fractal structure complex and self-similar.

As shown in Figure 3,with the decrease of the log-viscosity ratio between the displacing and displaced fluids and the enhancement of the impeding effect of the expelled fluid, the elongation of the finger-like structure and the appearance of a slight bifurcation of the main branch can be observed. With the relative decrease of the diffusion coefficient, the convective reaction starts to dominate in the competitive mechanism of diffusion and convection, driving the further complication of the fractal

structure and intensifying the occurrence of splitting. Increasing the injection rate of the replacement fluid will significantly expand the spreading area of the replacement interface, increasing the complexity of the finger-like structure region. The faster injection rate will lead to faster contact of the supplemental fluid with the dynamic interface, which will lead to increased interfacial destabilization and thus enhance the splitting action, thus increasing the number of "fingers".

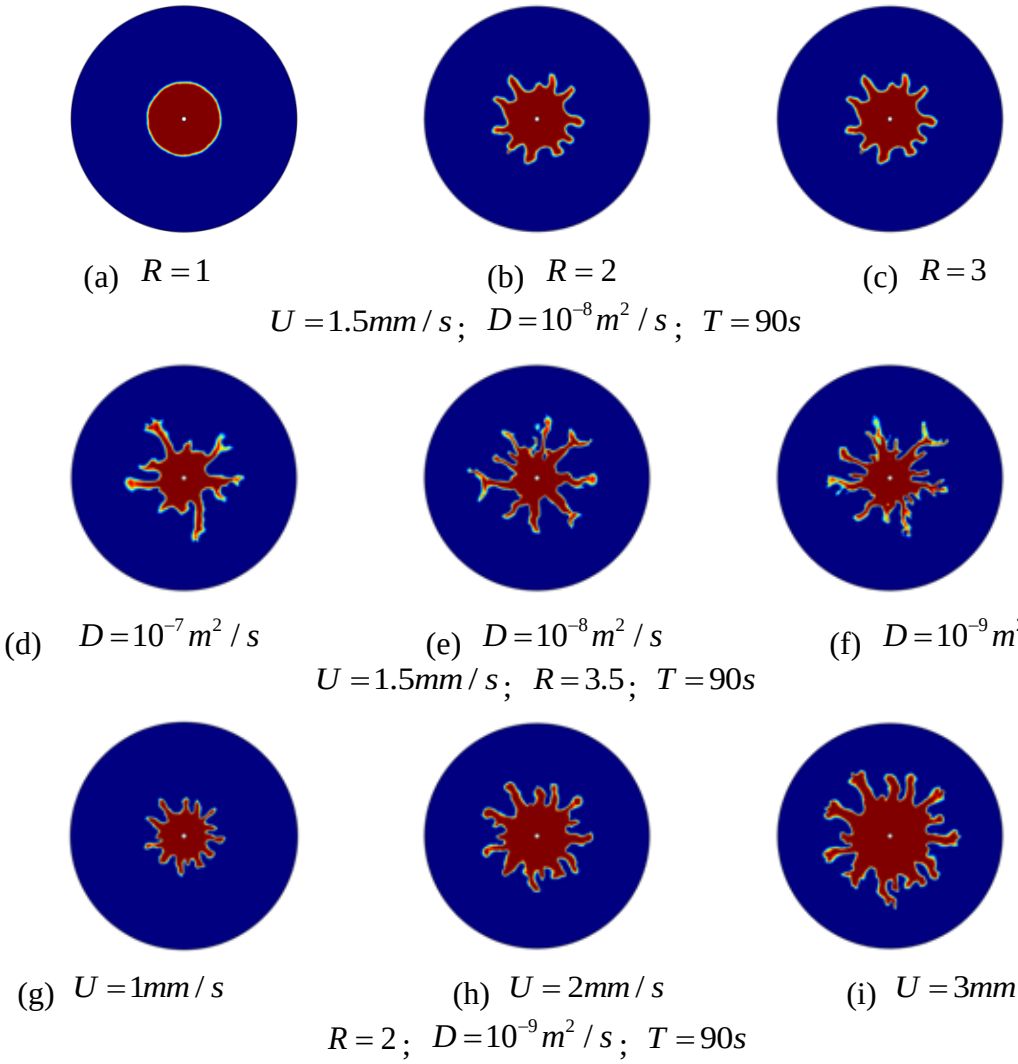

Figure 3: Fractal finger for variations in R, D and U

To further quantitatively analyze the effects of log-viscosity ratio, diffusion coefficient, and injection rate on the finger-like fractal structure, three metrics, namely, the boundary length, spreading area, and fractal dimensionality of the replacement fluid, will be used in this study to evaluate the effects of log-viscosity ratio, diffusion coefficient, and injection rate on the finger-like fractal structure in detail.

The length of the dynamic interface can be defined as[6]:

$$I(t)=\int_0^{L_y}\int_0^{L_x}\sqrt{\left(\frac{\partial c}{\partial x}\right)^2+\left(\frac{\partial c}{\partial y}\right)^2}\,dxdy \tag{7}$$

Figure 4 depicts images of the boundary length and spreading area for different diffusion coefficients D and injection rates of the replacement fluid U for a log-viscosity ratio R fixed

at 2. Figure 5 depicts images of the boundary length and spreading area for different log-viscosity ratios R and the injection rate of the replacement fluid U, for a diffusion coefficient fixed at $10^{-8}m^2/s$ at $T=90s$.

When the diffusion coefficient D was set to $10^{-7}m^2/s$, $10^{-8}m^2/s$, $10^{-9}m^2/s$, $10^{-10}m^2/s$,the consistency of the spreading area was high. However, the diffusion coefficient D was significantly reduced by taking 10^{-6}m^2/s,and the finger-entry phenomenon was never observed under this condition. The diffusion coefficient D was weakly reduced by taking $10^{-6}m^2/s$ to $10^{-7}m^2/s$, and no-finger-entry phenomenon was ever observed under this condition. When the diffusion coefficient D was smaller than $10^{-7}m^2/s$, the growth of the perturbation-enhanced fractal was significant.

When R is the independent variable, almost no fractal phenomenon occurs in the interval where R is taken as 0 to 1. Starting from R greater than 1, the perturbation and strengthened with the increase of R based on higher consistency of the spreading area, the boundary length increases gradually, indicating the complexity of the dynamic joint interface increases.

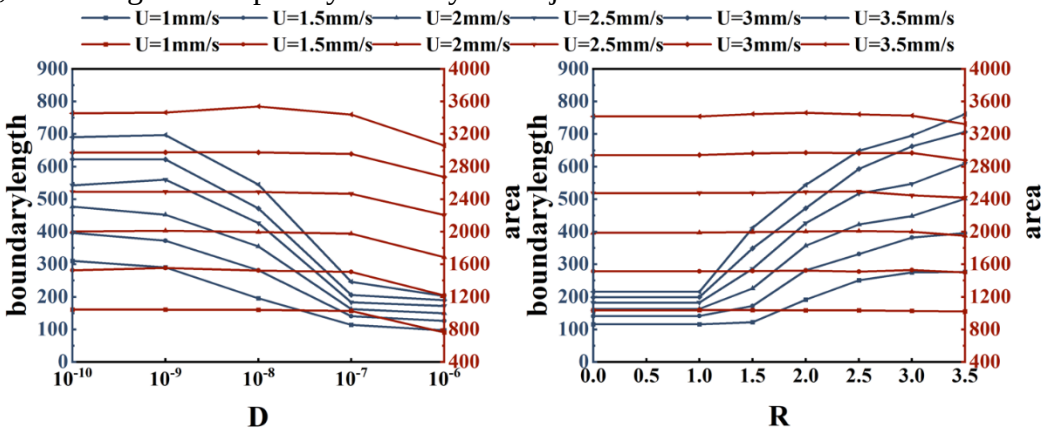

Figure 4: Effect of diffusion coefficient D on boundary length and spreading area (Left)

Figure 5: Effect of log-viscosity ratio R on boundary length and spread area (Right)

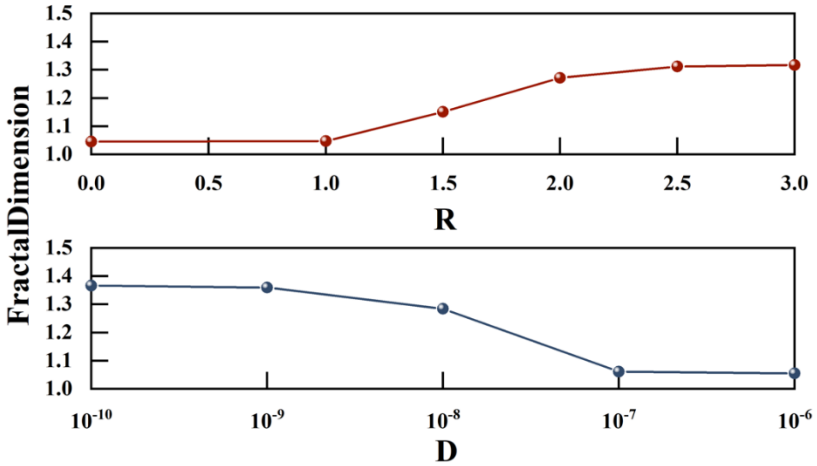

Figure 6: Effect of diffusion coefficient D and log-viscosity ratio R on the fractal dimension

Based on this framework, the image is imported into Matlab for edge extraction in this study.

Additionally, the box-counting method is utilized to calculate the Hausdorff fractal dimension of the finger, enabling further exploration of the complexity of the fractal structure using the following formula

$$D_f = -\lim_{r\to 0}\frac{\log N(r)}{\log r} \tag{8}$$

Where r is the radius of the box covering the fractal boundary line and $N(r)$ is the number of boxes covering the boundary line.

The variation of fractal dimension with diffusion coefficient D and log-viscosity ratio R is shown in Figure 6. In terms of the evolution of fractal morphology, the onset of the significant increase in fractal dimension with increasing log-viscosity ratio and decreasing diffusion coefficient is more in line with the onset of a significant increase in the length of the boundary. This data illustrates that the complexity of the fractal structure gradually increases, splitting starts to appear on the parent finger, and the splitting effect strengthens with the increase of the log-viscosity ratio and the decrease of the diffusion coefficient, and finally tends to stabilize.

Figure 7 demonstrates the fractal finger contour plots normalized for radius length and angle under the conditions of driving fluid injection flow rates of $1mm/s$, $2mm/s$ and $3mm/s$, respectively. The observations showed that the finger contours exhibited more consistent periodic fluctuation characteristics as the flow rate increased. Meanwhile, the boundary length and spreading area also show an increasing trend with increasing flow velocity, which reflects that the high-velocity fluid injection exacerbates the expansion phenomenon of the interface. In addition, bifurcation was observed at some of the fingertip locations, which may indicate that the increase in flow velocity has a certain effect on the morphology and complexity of the finger contour.

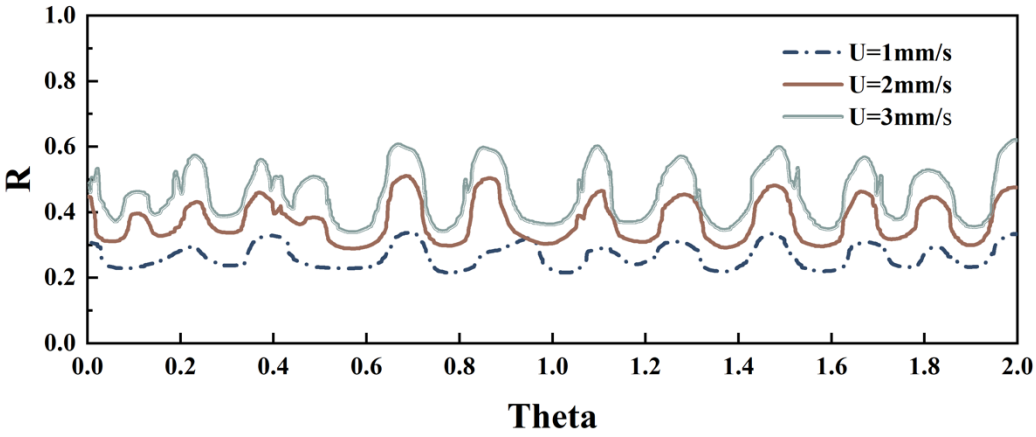

Figure 7: Fractal finger contours at different injection speeds

4. Conclusions

This paper conducts an in-depth analysis of the evolution of viscous fingering morphology and its influencing factors under an annular boundary through numerical simulations based on the Hele-Shaw model. The study specifically addresses three key parameters: the log-viscosity ratio, diffusion coefficient, and the injection rate of the displacing fluid. The results show that an increase in the viscosity ratio leads to more slender and branched finger structures, highlighting the significant impact of viscosity differences on the complexity of the morphology. Moreover, a lower diffusion coefficient introduces more complex fractal structures, underscoring the crucial role of diffusion in morphological development. Additionally, rapid injection of the displacing fluid enlarges the

interface spreading area and increases the complexity of the structure. This research integrates the two-phase Darcy's law and the dilute matter transfer model, offering new perspectives through quantitative analyses of boundary length, spreading area, and fractal dimension. The structural complexity was further quantified using Matlab image processing and the box-counting method, validating the fractal dimension as an effective metric for assessing the complexity of fluid interface morphology. These findings not only deepen the theoretical understanding of the viscous fingering phenomenon but also provide guidance for fluid control and optimization. Future studies will explore additional influencing factors and their interactions with morphological evolution, aiming to enhance understanding through experimental validation and multiscale simulation.

References

[1] Saffman P G, Taylor G I. The penetration of a fluid into a porous medium or Hele-Shaw cell containing a more viscous liquid [J]. Proceedings of the Royal Society of London Series A Mathematical and Physical Sciences, 1958, 245(1242): 312-329.

[2] Pramanik S, Mishra M. Comparison of Korteweg stresses effect on the fingering instability of higher or less viscous miscible slices: Linear stability analysis [J]. Chemical Engineering Science, 2014, 110: 144-152.

[3] Deki Y F, Nagatsu Y, Mishra M, et al. Numerical study of the effect of Peclet number on miscible viscous fingering with effective interfacial tension [J]. Journal of Fluid Mechanics, 2023, 965: A22.

[4] Nand S, Sharma V, Das S K, et al. Effect of Hele–Shaw cell gap on radial viscous fingering [J]. Scientific Reports, 2022, 12(1): 18967.

[5] Sharma V, Othman H B, Nagatsu Y, et al. Viscous fingering of miscible annular ring [J]. Journal of Fluid Mechanics, 2021, 916: A14.

[6] Mishra M, Martin M, De Wit A. Differences in miscible viscous fingering of finite width slices with positive or negative log-mobility ratio [J]. Physical Review E, 2008, 78(6): 066306.